NDT&E International 55 (2013) 96–101

Contents lists available at SciVerse ScienceDirect

NDT&E International

journal homepage: www.elsevier.com/locate/ndteint

Discussion on modeling of thermal fatigue cracks in numerical simulation based on eddy current signals

Jing Wang [a,*], Noritaka Yusa [b], Hongliang Pan [a], Mika Kemppainen [c], Iikka Virkkunen [c], Hidetoshi Hashizume [b]

[a] School of Mechanical and Power Engineering, East China University of Science and Technology, 130 Meilong, Xuhui, Shanghai 200237, China
[b] Department of Quantum Science and Energy Engineering, Graduate School of Engineering, Tohoku University, 6-6 Aramaki Aza Aoba, Aoba-Ku, Sendai, Miyagi 980-8579, Japan
[c] Trueflaw Ltd., Tillinmäentie 3, tila A113, 02330 Espoo, Finland

ARTICLE INFO

Article history:
Received 15 September 2012
Received in revised form
19 December 2012
Accepted 6 January 2013
Available online 23 January 2013

Keywords:
Thermal fatigue crack
Numerical modeling
Finite element method
Eddy current testing

ABSTRACT

This study evaluates modeling of thermal fatigue cracks by the finite element method from the view point of eddy current testing. Five artificial thermal fatigue cracks introduced into type 304 stainless steel plates were prepared for the research. Eddy current signals were gathered by a differential type plus point probe and subsequent destructive tests were performed to confirm the true profiles of the cracks. Numerical simulation based on the results of eddy current testing and destructive tests were carried out to show how the thermal fatigue cracks should be modeled in numerical simulations. The results of the numerical simulations revealed that thermal fatigue cracks tend to be much less conductive than stress corrosion cracks if they are assumed to have uniform conductivity inside. The results also imply that taking consideration of magnetization induced by the thermal fatigue process enables eddy current signals to be analyzed more quantitatively.

1. Introduction

Thermal fatigue is attributed to uneven temperature distribution, and inevitably occurs in components where temperatures alternate, e.g., a T-joint with mixture of hot and cold fluids [1]. With the cumulative damage of thermal fatigue, cracks of the type called the thermal fatigue crack (TFC) are widely generated in industrial processes. Therefore, carrying out active non-destructive inspection for TFCs has significant importance for safety and for ensuring continuity of industrial production.

In general, TFCs have a small crack opening and many branches [2]. Whereas ultrasonic testing (UT) is the most popular method for sizing defects of components [3,4], the accuracy of measurement of UT tends to be affected by the minute properties of the crack [5,6]. Furthermore carrying out UT is time-consuming, and utilization of a couplant is necessary. These facts indicate that the application of non-ultrasonic-based nondestructive testing together with UT should provide more quantitative evaluation of TFCs.

Eddy current testing (ECT) is one of the most promising non-destructive testing methods from this point of view. Advanced computational physics for electromagnetic fields enable quantitative evaluation of crack profiles from ECT signals [7,8]; a few studies have even reported success in quantitative evaluation of stress corrosion cracks (SCC) [9,10]. However, recent studies have pointed out that the accuracy of evaluation strongly depends on how a crack is modeled [11–15]. This indicates that evaluating the modeling of TFCs is essential to discuss the applicability of ECT to the evaluation of TFCs. However, studies on the nondestructive evaluation of TFCs have been carried out mainly from the viewpoint of UT [16,17].

This study is conducted on the basis of the above background and aims to evaluate the modeling of TFCs in an eddy current numerical simulation. Five TFCs artificially introduced into austenitic stainless steel plates were investigated. The eddy current testing utilized a plus point probe driven at three frequencies. Subsequent destructive tests were carried out to reveal the profile of the TFCs. Based on the results of the eddy current testing and destructive tests, modeling of TFCs was evaluated in numerical simulations.

2. Materials and methods

2.1. Preparation of thermal fatigue crack samples

Three type 304 austenitic stainless steel plates were prepared for this study. Each plate measured 250 mm long, 150 mm wide, 25 mm thick and had a chemical composition listed in Table 1. Thermal fatigue loading was introduced by alternate heating and

* Corresponding author. Tel.: +81 22 795 7906; fax: +81 22 795 6319.
E-mail addresses: jwang@karma.qse.tohoku.ac.jp, jingwang8604@gmail.com (J. Wang).

0963-8695/$ - see front matter © 2013 Elsevier Ltd. All rights reserved.
http://dx.doi.org/10.1016/j.ndteint.2013.01.012

cooling. Heating was applied with high frequency induction, and cooling with a water spray. Maximum temperatures used were below 400 degrees, and minimum temperatures were around 10 degrees. Two TFCs were introduced to each of two of the plates, and one TFC to the third. Hereafter, these five cracks are denoted as TFC1-5. These artificial TFCs were regarded as favorable representatives of service-induced TFCs since previous study has proved that TFCs produced by controlled thermal fatigue loading have quite similar performance to service-induced forms, according to results of metallographic analysis and UT [16,17].

2.2. Eddy current testing and destructive tests

Eddy current testing was conducted to measure eddy current signals using a differential type plus point probe illustrated in Fig. 1. The plus point probe consists of two differentially connected square coils with inner lengths, thicknesses, and widths of 5.0, 3.0, and 0.2 mm, respectively. Since the depths of the flaws were estimated to be around 4 mm and an earlier study demonstrated eddy current signals gathered using a differential plus point probe shows dependency on flaw depth up whose depth is up to the twice of the depth of penetration [14], this study adopted an exciting frequency of 50 kHz that provides a skin depth of approximately 1.94 mm, In order to discuss the dependency of modeling on frequency two additional frequencies of 100 and 400 kHz were also utilized. An XYZ stage controlled by a PC positioned the probe during the inspection, and the probe scanned along lines parallel to a crack.

The specimens were destroyed to reveal the true profile of the TFCs after the eddy current testing. The destructive tests evaluated both the cross-section at the center of the cracks and the boundary profiles to confirm the three-dimensional geometry of the cracks.

Table 1
Chemical composition of the plates.

	C	Si	Mn	P	S	Ni	Cr	Co
Content	0.019	0.420	1.750	0.028	0.001	8.170	18.360	0.110

Unit: %.

2.3. Numerical simulations

Finite element simulations were performed to show the numerical modeling of TFCs from the viewpoint of eddy current testing. The simulations modeled a TFC as a planar region with a constant width, and evaluated the electrical properties of the crack that reproduced the measured eddy current signals. The difference between the measured and simulated signals was calculated by

$$\varepsilon = \sum_{i=1}^{5} |Z_i^{\mathrm{mea}} - Z_i^{\mathrm{sim}}| \quad (1)$$

where Z^{mea} and Z^{sim} denote measured and simulated eddy current signals, respectively and subscript i denotes signals measured at the ith scanning point. Thus, comparison between signals of measurement and simulation were carried out by considering the trajectory of signals when the probe scanned directly above the crack. In the study, a total of five scanning points were considered. The maximum value of trajectory could be gathered at the third scanning point; the other four scanning points were uniformly and symmetrically distributed beside the third

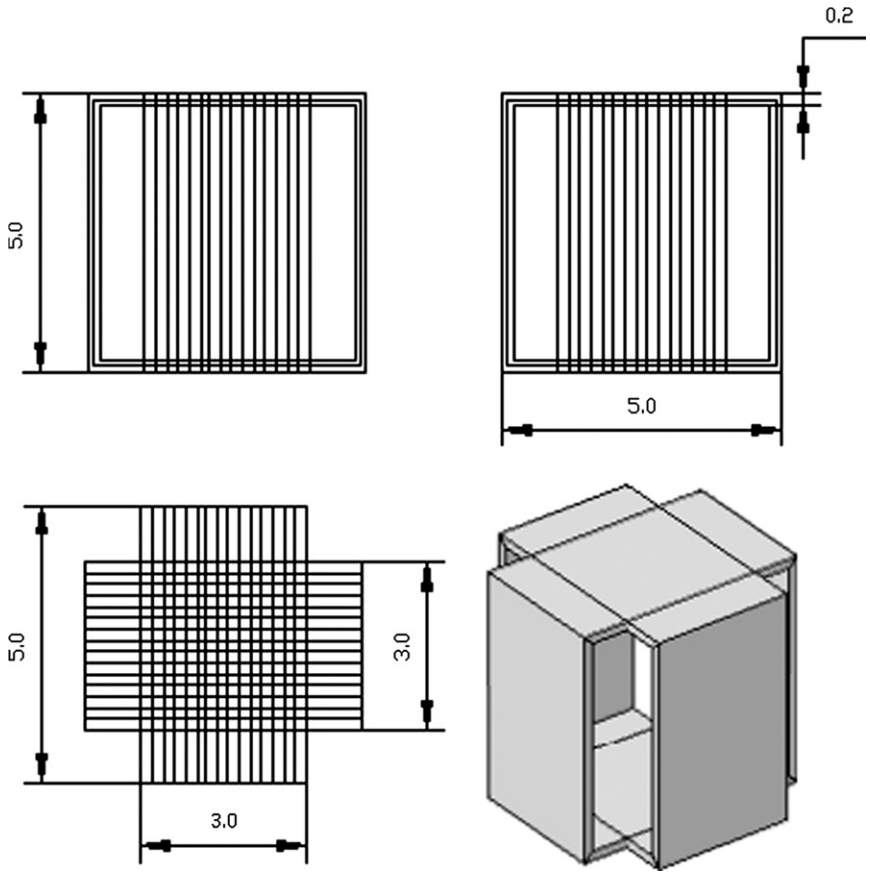

Fig. 1. The differential type plus point probe utilized to measure eddy current signals.

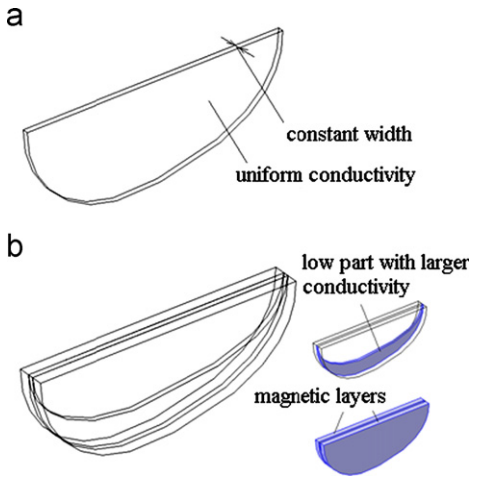

Fig. 2. Model of thermal fatigue in numerical simulation: (a) Model A with constant width and uniform conductivity; (b) model B, considering electromagnetic variation in the vicinity of a thermal fatigue crack to illustrate conductive variation.

scanning point so that the signal trend could be clearly expressed by the values given at these points.

The simulations were conducted by commercial software, Comsol Multiphysics and its AC/DC module. The governing equation is

$$(j\omega\sigma-\omega^2\varepsilon)A+\nabla\times(\mu^{-1}\nabla\times A)=J_e \quad (2)$$

where ω is the angular frequency, σ is the conductivity, ε is the permittivity, A is the magnetic vector potential, μ is the permeability and J_e is the current density of the exciter. A curl element was utilized in the numerical model. The size of the computational domain was $400\times400\times400$ mm. The boundary condition was imposed so that the tangential component of the magnetic vector potential was zero. The total number of elements in the model was about 200,000. The mesh was sufficiently fine so that the error caused by the mesh was only 0.08% of the signal.

Fig. 2 illustrates the two numerical models utilized in this study. Both the models have a constant width, and the boundary profile of a crack is as correctly modeled as possible on the basis of the results of the destructive test. Model A, shown in Fig. 2(a) models a crack as a region with a constant width and uniform conductivity inside. The width was set to be as 0.01, 0.02, 0.05, 0.10, 0.20, 0.50, or 1.00 mm; the conductivity was assumed to be 0.0, 0.1, 0.2, 0.5, 1.0, 2.0, 5.0, or 10.0% of the base material's conductivity (1.35 MS/m).

Another model, model B shown in Fig. 2(b), assumes that the conductivity in a deep part of a crack is larger than that near the surface [18]. The upper half of a crack has a constant width and uniform conductivity identical to the ones that minimized Eq. (1) using model A. The adoption of optimized width and conductivity in the upper half of a crack is related to two reasons. First minimum initial difference between measured and simulated signal could be reached using optimized width and conductivity compared with other widths and conductivities. Furthermore, the optimized width is the most similar one to the result of optical microscope tests. The lower half of a crack has, in contrast, greater conductivity, whereas the width is the same as that of the upper half of the crack. The conductivity of the lower half was set to be 0.5, 1.0, 2.0, 5.0, or 10.0% of the base material's conductivity. The possibility of magnetization induced due to the thermal fatigue process, in the vicinity of a TFC, was modeled by two magnetic layers beside the crack. These two layers had the same boundary profile with the flaw and their conductivities were same with that of the base material. The relative permeability and width of the layers were assumed to be 1, 2, 3, 4, 5 and 1, 2, 5, 10 times of the width that minimized Eq. (1) using model A, respectively. Furthermore, these layers had identical conductivity and relative permeability for each simulation.

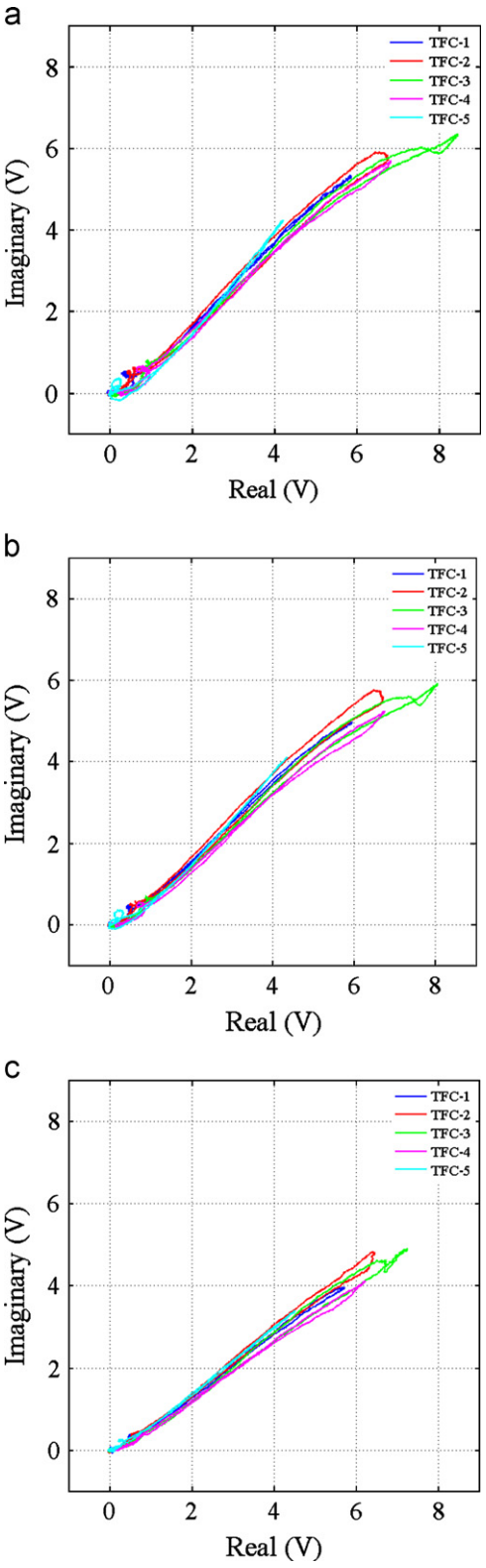

Fig. 3. Trajectories of the eddy current signals measured using the plus point probe. (a) 50 kHz, (b) 100 kHz, (c) 400 kHz.

3. Results and discussion

The trajectories of the eddy current signals measured by the eddy current instruments are shown in Fig. 3. The signals shown in the figure were those measured along a scanning line where the maximum signal was obtained, and they were all calibrated so that the maximum signal due to an artificial rectangular slit of 20.0 mm long, 0.5 mm wide, and 5.0 mm deep had an amplitude of 10 V and phase of 45 degrees. Signals of simulation in this paper were also calibrated by the same slit.

The results of optical microscope tests are shown in Fig. 4. This reveals that all the cracks are generated in one direction except TFC-5. An obvious cluster is shown in Fig. 4(e). An example of cross-sectional profiles of one of the cracks, TFC-3, is presented in Fig. 5. Pictures with higher resolutions are available at http://jsm.or.jp/jsm/at/scc/index_eng.htm. Profiles of other cracks did not differ significantly from those in the figure. That is, no cluster was observed in the direction of the depth of a crack. Fig. 6 demonstrates a geometric model of a numerical simulation. The boundary profiles of the cracks, namely the crack profile on the plane parallel to the crack, revealed by the destructive tests are also shown in Fig. 6. Table 2 summarizes the maximum lengths and depths of the cracks evaluated from the results of optical microscope tests and destructive tests.

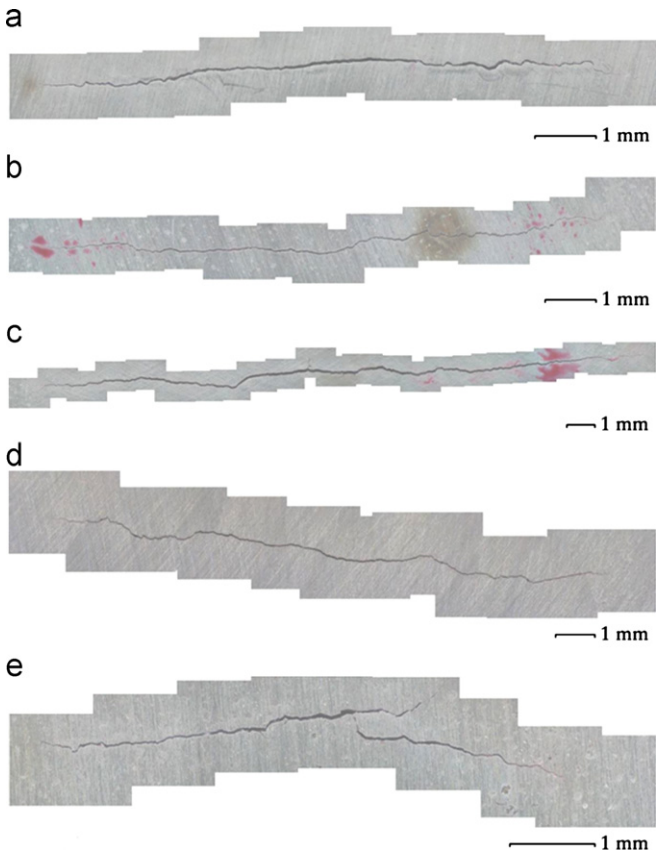

Fig. 4. Results of optical microscope tests. (a) TFC-1; (b) TFC-2; (c) TFC-3; (d) TFC-4; (e) TFC-5.

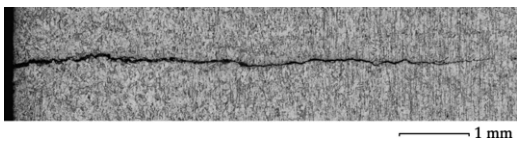

Fig. 5. Examples of the cross-sectional profile of the crack (TFC-3).

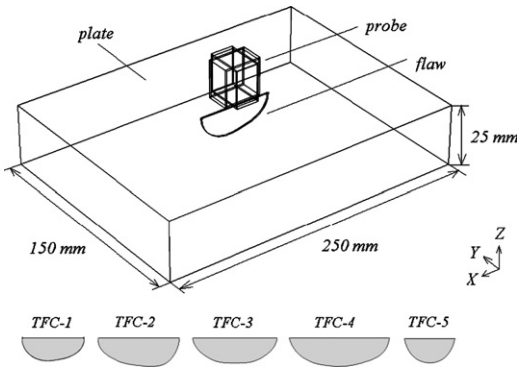

Fig. 6. Geometric model of simulation. Boundary profiles of the cracks are revealed by a destructive test.

Table 2
Maximum lengths and depths of the cracks.

	Max. length (mm)	Max. depth (mm)
TFC-1	9.7	3.5
TFC-2	11.7	4.1
TFC-3	22.1	6.5
TFC-4	14.4	4.1
TFC-5	6.5	3.1

Table 3
Evaluated crack parameters without considering electromagnetic variation in the vicinity of the TFC (model A).

Crack	Freq. (kHz)	Conductivity (%)[a]	Width (mm)	ε
TFC-1	50	0.0	0.01	1.75
	100	0.1	0.10	1.48
	400	0.1	0.10	1.14
TFC-2	50	0.0	0.01	2.79
	100	0.0	0.01	1.57
	400	0.0	0.05	1.45
TFC-3	50	0.1	0.10	2.15
	100	0.1	0.10	1.82
	400	0.2	0.20	2.55
TFC-4	50	0.0	0.01	3.16
	100	0.1	0.10	2.62
	400	0.1	0.10	2.74
TFC-5	50	0.1	0.05	2.11
	100	0.2	0.05	1.77
	400	2.0	0.50	1.68

[a] Conductivity with respect to the base material.

The conductivity and width of the cracks minimizing Eq. (1) using model A are summarized in Table 3, together with the value of ε that the conductivity and width provide. The values of conductivity show that a TFC is much less conductive than an SCC, as earlier publications have proved [15,19]. However, the conductivity of TFC-5 is relatively higher, especially when a frequency of 400 kHz is employed. The most plausible reason would be that the cluster of TFC-5, as Fig. 4(e) shows, increases the area of the contact between the fracture surfaces of cracks.

The results of Table 3 indicate that the conductivity and width tend to become larger with the increase in frequency. Whereas it is plausible that this is due to the shallower depth of penetration and larger crack opening near the surface of plate; validations using more number of specimens are indispensable for further discussion. It should be noted, however, the resistance defined as width divided

Table 4
Evaluated crack parameters considering electromagnetic variation in the vicinity of TFC (model B) when a frequency of 50 kHz is used.

Crack	Conductivity[a] of conductive edge	Width of magnetic layer (mm)	Relative permeability of magnetic layer	ε
TFC-1	1.0	0.1	4	1.48
TFC-2	5.0	0.1	5	2.53
TFC-3	10.0	1.0	2	1.58
TFC-4	5.0	0.1	5	2.89
TFC-5	5.0	0.5	2	1.66

[a] Conductivity with respect to the base material.

by the conductivity is almost unchanged, which agrees well with the previous study on modeling of SCC [15,19].

Table 4 shows results obtained by considering electromagnetic variation in the vicinity of TFCs when 50 kHz was utilized, namely results obtained by model B. The fact that the lower half of a crack was more conductive would be due to the partial closure. The closure is assumed to be caused by the tortuosity of the crack path and compression stress around the tip of the crack [20,21]. A real crack opening would be smaller than the crack opening demonstrated by metallographic analysis in Fig. 5 since etching would increase the crack opening by rounding its fracture surface. It has been shown that the width of the magnetic layer tends to increase along with the size of the crack opening. In

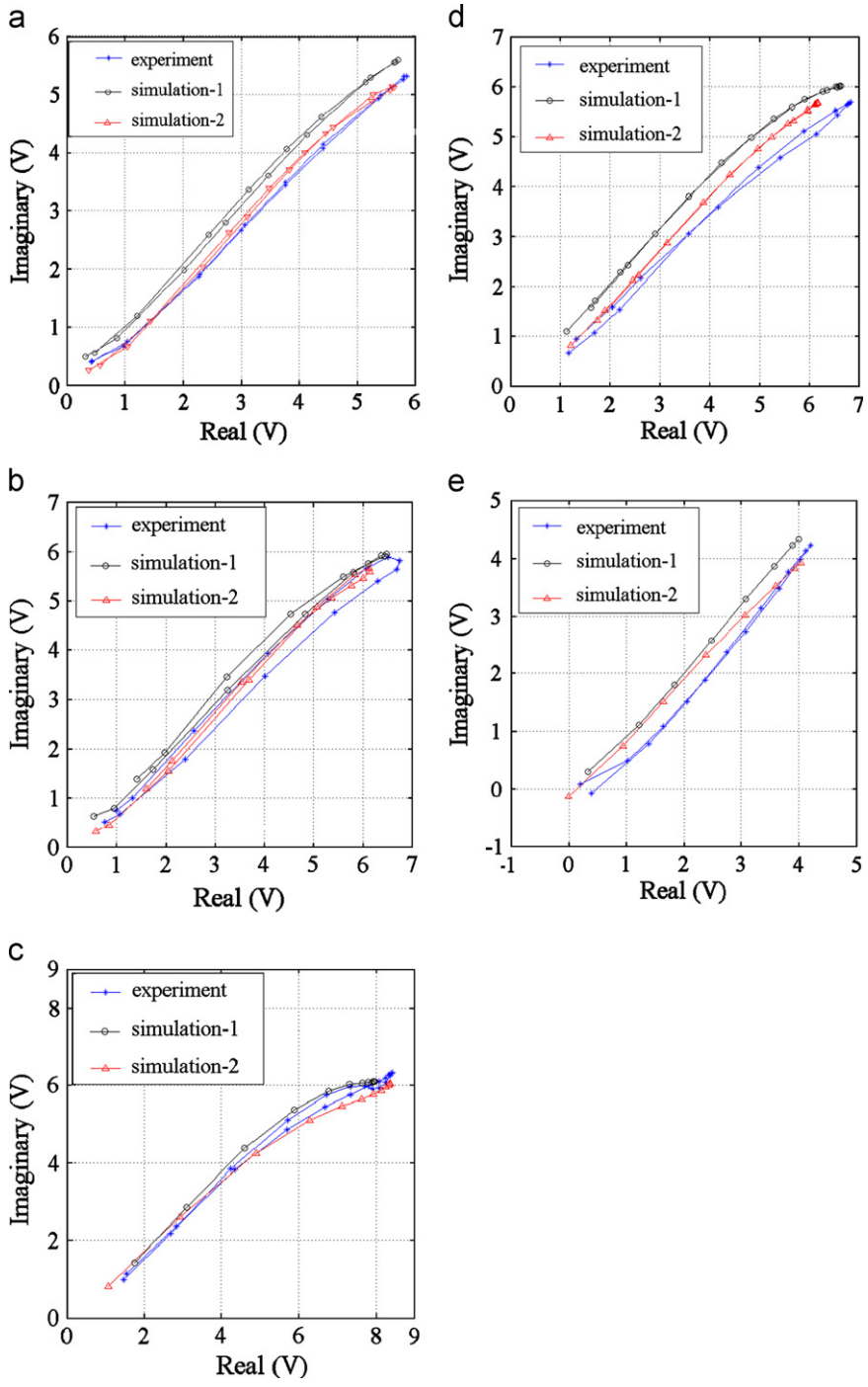

Fig. 7. Trajectories of the measured signal and simulated signal generated by two models of TFC when a frequency of 50 kHz is used. Simulation-1 presents the results of modeling TFC by model A. Simulation-2 presents the results of modeling TFC by model B. (a) TFC-1; (b) TFC-2; (c) TFC-3; (d) TFC-4; (e) TFC-5.

practice, magnetization is caused by plastic deformation during the propagation of the crack since the base material is type 304 austenitic stainless steel. It has been demonstrated that type 304 austenitic stainless steel becomes magnetic after the generation of plastic deformation [22]. This reasonably explains why the range of the magnetic layer is related to the size of the crack.

Fig. 7 illustrates the trajectories of the measured signal and simulated signal produced by the above two models of TFC at a frequency of 50 kHz. The results from more than five scanning points are shown in the figure for better presentation of the trajectories. Combined with the values of ε shown in Tables 2 and 3, they indicate that modeling of TFC could be developed to a certain extent by considering magnetizations induced by the thermal fatigue process. However, the result of TFC-3 in Fig. 7 does not show obvious improvement in reconstruction of the eddy current signal. That means it is not always necessary to consider magnetization of modeling of TFCs for more accurate reconstruction.

4. Conclusion

This study evaluated modeling of the TFC in a numerical simulation from the viewpoint of eddy current testing. Five artificial TFCs introduced into type 304 austenitic stainless steel plates were prepared for the research. Signals were gathered by a differential type plus point probe using several frequencies.

Each crack was simulated as two kinds of models. Both models had a constant width and true profile revealed by destructive test. Model A had uniform conductivity. Then, the conductivity and width of the TFC were evaluated by this model. The results demonstrated that the resistance defined as width divided by the conductivity is almost unchanged, even though the conductivity and width become larger with an increase in frequency. The values of the conductivity indicate that TFC is much less conductive than a stress corrosion crack, and thus the latter should be modeled as a more conductive region according to previous research.

Furthermore, model B, considering magnetization induced due to the thermal fatigue process was also used to simulate a TFC. The more conductive lower part of the TFC would be caused by the partial closure and compression stress around the tip of the crack. The magnetic layer would be due to the plastic deformation since the base material was a type 304 austenitic stainless steel. In general, modeling of TFCs could be developed further by considering magnetizations induced by the thermal fatigue process. However, one of the reconstructive results in Fig. 7 indicates that considering magnetization in the vicinity of a TFC does not always enable more accurate reconstruction.

Acknowledgment

This study was supported by a project launched by the Japan Society of Maintenology aiming at the enhancement of NDT & E of stress corrosion cracks [23]. The results of optical microscope tests can be found on the website http://jsm.or.jp/jsm/at/scc/index_eng.htm.

References

[1] Chapuliot S, Gourdin C, Payen T, Magnaud JP, Monavon A. Hydro-Thermal-Mechanical analysis of thermal fatigue in a mixing tee. Nucl Eng Des 2005;235:575–96.
[2] Wale, J. Crack characterization for in-service inspection planning—an update. SKI reference 14.43-200543105, ISRN SKI-R-06/24-SE, SKI, Stockholm, Sweden; 2006: 24. ISSN 1104-1374.
[3] Whittle M. A review of worldwide practice and experience in the qualification of ultrasonic inspections of nuclear components over the past two decades. Insight: Non-Destr Test Cond Monit 2009;51(3):140–50.
[4] Ahmed S, Saka M. A new ultrasonic angle-beam technique for sensitive evaluation of closed cracks. NDT&E Int 1999;33:261–71.
[5] Saka M, Salam Akanda M. Ultrasonic measurement of the crack depth and crack opening stress intensity factor under a no-load condition. J Nondestr Eval 2004;23(2):49–63.
[6] Kemppainen M, Virkkumen I, Packalen T, Sillanpaa J, Paussu R. Importance of crack opening in UT inspection qualification. In: Proceedings of the sixth international conference on NDE in relation to structural integrity for nuclear and pressurised components, 8–19 October: Budapest, Hungary; 2007. p. 93–105.
[7] Bowler JR. Review of eddy current inversion with application to nondestructive evaluation. Int J Appl Electromagn Mech 1997;8(1):3–16.
[8] Auld BA, Moulder JC. Review of advances in quantitative eddy current nondestructive evaluation. J Nondestr Eval 1999;18(1):3–36.
[9] Yusa N, Chen Z, Miya K. Sizing of stress corrosion cracking on austenitic stainless piping in a nuclear power plant from eddy current NDT signals. Nondestr Testing Eval 2005;20(2):103–14.
[10] Yusa N, Chen Z, Miya K, Uchimoto T, Takagi T. Large-scale parallel computation for the reconstruction of natural stress corrosion cracks from eddy current testing signals. NDT&E Int 2003;36:449–59.
[11] Yusa N, Perrin S, Mizumo K, Miya K. Numerical modeling of general cracks from the viewpoint of eddy current simulations. NDT&E Int 2007;40:577–83.
[12] Badics Z, Matsumoto Y, Aoki K, Nakayasu F, Kurokawa A. Finite element models of stress corrosion cracks (SCC) in 3-D eddy current NDE problem. In: Collins R, Dover WD, Bowler JR, Miya K, editors. Nondestructive testing of materials. IOS Press; 1995. p. 21–9.
[13] Chen Z, Aoto K, Miya K. Reconstruction of cracks with physical closure form signals of eddy current testing. IEEE Trans Magn 2000;36:1018–22.
[14] Yusa N, Huang H, Miya K. Numerical evaluation of the ill-posedness of eddy current problems to size real cracks. NDT&E Int 2007;40:185–91.
[15] Yusa N, Miya K. Discussion on the equivalent conductivity and resistance of stress corrosion cracks in eddy current simulations. NDT&E Int 2009;42:9–15.
[16] Kemppainen M, Virkkunen I, Pitkänen J, Paussu R, Hänninen H. Advanced flaw production method for in-service inspection qualification mock-ups. Nucl Eng Des 2003;224:105–17.
[17] Kemppainen M, Virkkunen I. Crack characteristics and their importance to NDE. J Nondestr Eval 2011;30(3):143–57.
[18] Yusa N, Hashizume H. Four-terminal measurement of the distribution of electrical resistance across stress corrosion cracking. NDT&E Int 2011;44:544–6.
[19] Yusa N, Hashizume H. Evaluation of stress corrosion cracking as a function of its resistance to eddy currents. Nucl Eng Des 2009;239:2713–8.
[20] Kane A, Doquet V. Problems related to thermal fatigue of stainless steel: interactions of orthogonal cracks networks under biaxial tension and influence of stress biaxiality on 3D mode I crack growth. In: 15th European conference on fracture, ECF15: Stockholm France; 2004.
[21] Marci G, Packman P. The effect of the plastic wake zone on the conditions for fatigue crack propagation. Int J Fracture 1980;16(2):133–53.
[22] Li H, Chen Z, Li Y, Takagi T, Uchimoto T, Chigusa N, et al. Dependence of deformation-induced magnetic field on plastic deformation for SUS304 stainless steel. Int J Appl Electromagn Mech 2012;38:17–26.
[23] Yusa N, Miya K, Komura I, Chen Z. A project aiming at the enhancement of NDT&E of stress corrosion cracking. Int J Appl Electromagn Mech 2012;33:1587–90.